

See discussions, stats, and author profiles for this publication at: <https://www.researchgate.net/publication/267871142>

# Probing the Nanostructure, Interfacial Interaction, and Dynamics of Chitosan-Based Nanoparticles by Multiscale Solid-State NMR

ARTICLE in ACS APPLIED MATERIALS & INTERFACES · NOVEMBER 2014

Impact Factor: 6.72 · DOI: 10.1021/am5064052 · Source: PubMed

---

READS

81

## 6 AUTHORS, INCLUDING:



Fenfen Wang

Nankai University

2 PUBLICATIONS 0 CITATIONS

[SEE PROFILE](#)



Rongchun Zhang

University of Michigan

27 PUBLICATIONS 123 CITATIONS

[SEE PROFILE](#)



Pingchuan Sun

Nankai University

119 PUBLICATIONS 1,544 CITATIONS

[SEE PROFILE](#)



An-Chang Shi

McMaster University

232 PUBLICATIONS 3,592 CITATIONS

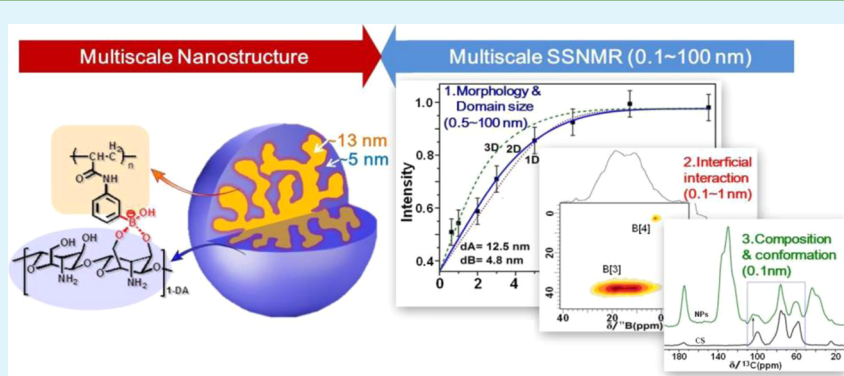
[SEE PROFILE](#)

# Probing the Nanostructure, Interfacial Interaction, and Dynamics of Chitosan-Based Nanoparticles by Multiscale Solid-State NMR

Fenfen Wang,<sup>†</sup> Rongchun Zhang,<sup>†</sup> Qiang Wu,<sup>†</sup> Tiehong Chen,<sup>†</sup> Pingchuan Sun,<sup>\*,†</sup> and An-Chang Shi<sup>‡</sup>

<sup>†</sup>Key Laboratory of Functional Polymer Materials of the Ministry of Education and College of Chemistry, State Key Laboratory of Medicinal Chemical Biology, Nankai University and Collaborative Innovation Center of Chemical Science and Engineering (Tianjin), Tianjin 300071, China

<sup>‡</sup>Department of Physics and Astronomy, McMaster University, Hamilton, Ontario L8S 4M1, Canada



**ABSTRACT:** Chitosan-based nanoparticles (NPs) are widely used in drug and gene delivery, therapy, and medical imaging, but a molecular-level understanding of the internal morphology and nanostructure size, interface, and dynamics, which is critical for building fundamental knowledge for the precise design and efficient biological application of the NPs, remains a great challenge. Therefore, the availability of a multiscale (0.1–100 nm) and nondestructive analytical technique for examining such NPs is of great importance for nanotechnology. Herein, we present a new multiscale solid-state NMR approach to achieve this goal for the investigation of chitosan–poly(*N*-3-acrylamidophenylboronic acid) NPs. First, a recently developed <sup>13</sup>C multiple cross-polarization magic-angle spinning (MAS) method enabled fast quantitative determination of the NPs’ composition and detection of conformational changes in chitosan. Then, using an improved <sup>1</sup>H spin-diffusion method with <sup>13</sup>C detection and theoretical simulations, the internal morphology and nanostructure size were quantitatively determined. The interfacial coordinated interaction between chitosan and phenylboronic acid was revealed by one-dimensional MAS and two-dimensional (2D) triple-quantum MAS <sup>11</sup>B NMR. Finally, dynamic-editing <sup>13</sup>C MAS and 2D <sup>13</sup>C–<sup>1</sup>H wide-line separation experiments provided details regarding the componential dynamics of the NPs in the solid and swollen states. On the basis of these NMR results, a model of the unique nanostructure, interfacial interaction, and componential dynamics of the NPs was proposed.

**KEYWORDS:** nanoparticles, chitosan, coordinated interaction, morphology, solid-state NMR

## 1. INTRODUCTION

Nanoparticles (NPs) based on biopolymers, such as the cationic polysaccharide chitosan, have attracted increasing interest in drug and gene delivery,<sup>1–3</sup> biosensors,<sup>4</sup> therapies,<sup>5</sup> and molecular imaging<sup>6</sup> because of their excellent biocompatibility and biodegradability. In particular, hybrid biopolymer-based NPs with two or more components exhibit superior performance and enjoy widespread application.<sup>7–13</sup> For example, boronic acid-containing polymers can react with the diol groups of saccharides to form the cyclic boronate ester that is widely used in preparing boron-rich, biopolymer-based NPs.<sup>8</sup> Recently, novel boronic acid-rich chitosan nanoparticles were successfully prepared and used for doxorubicin delivery;<sup>9,10</sup> the incorporation of boronic acid into chitosan NPs provides the NPs with good cellular uptake properties and improved stability.<sup>9</sup> Hybrid biopolymer-based NPs usually exhibit

complex internal morphology, interfacial interaction, and componential dynamics, which can sensitively alter the macroscopic properties of the NPs over a wide range. Therefore, an understanding of the nanostructure and dynamics of these NPs is crucial for their biological application.<sup>10</sup> For example, it was previously observed that the proportion of chitosan in NPs has a significant effect on controlling the pH response and the target drug delivery performance of NPs.<sup>9</sup> Functional groups<sup>5</sup> and surface charge<sup>14</sup> have also been observed to affect the cellular uptake and intracellular trafficking of chitosan-based NPs. The drug loading and drug encapsulation efficiency of NPs have been attributed to the

Received: September 17, 2014

Accepted: November 5, 2014

Published: November 5, 2014

hydrophobic core and hydrophilic shell of the nanoparticles.<sup>15</sup> The coordination type and content of phenylboronic acid units, in addition to the coordinated interaction between different components, are also crucial for the recognition ability and target drug delivery of phenylboronic acid-containing NPs.<sup>9</sup> In addition, the segmental dynamics of NPs are also quite important for controlling the diffusion efficiency of drugs enclosed in such NPs.<sup>16</sup>

Despite numerous advances,<sup>17–19</sup> multiscale characterization of the nanostructure of hybrid biopolymer-based NPs on the scale of 0.1–100 nm remains a great challenge. First, although the quantification of composition of hybrid NPs is critical, there is still no convenient quantitative method based on traditional liquid or solid-state NMR that can be used to this end because the NPs are usually insoluble. Second, the internal morphology of NPs is usually observed by transmission electron microscopy (TEM), but this method is limited by the staining quality of different phases. In addition, scattering methods are only sufficiently sensitive for samples with a periodic structure and depend on the electronic density contrast of different phases. The above-mentioned shortcomings largely limit the precise design and preparation, in addition to the efficient biological application, of such NPs.

Solid-state NMR (SSNMR) spectroscopy is a nondestructive and powerful technique for studying the multiscale structure, interfacial interaction, and dynamics of multiphase polymers at lengths ranging from the atomic level to approximately 100 nm.<sup>20–24</sup> The <sup>1</sup>H double-quantum and dipolar filter with spin-diffusion technique was successfully applied to characterize the morphologies and interfaces of bulk and core–shell polymers, with a remarkable dynamic contrast of the two domains.<sup>25,26</sup> A novel solid-state NMR approach based on <sup>1</sup>H spin diffusion with X-nucleus (<sup>13</sup>C, <sup>31</sup>P, <sup>15</sup>N) detection was also proposed for investigation of the nanostructure of membrane proteins.<sup>27</sup> Recently, a new method was reported to yield quantitative <sup>13</sup>C CPMAS NMR spectra of organic solid materials with good a signal-to-noise ratio.<sup>28</sup> For materials containing quadrupolar nuclei, such as <sup>11</sup>B, 1D MAS has been used to identify the coordination of phenyl-boronic acid in NPs.<sup>8</sup> Simultaneously, the advanced <sup>11</sup>B 3QMAS technique<sup>29,30</sup> is capable of providing high-resolution spectra to reveal complex boronic sites and interfacial interactions in polymer blends containing phenyl-boronic acid. Moreover, 2D <sup>1</sup>H–<sup>1</sup>H nuclear overhauser enhancement spectroscopy (NOESY) has been used to probe the intermolecular interactions of some NPs<sup>31</sup> as well as the interaction between dendrimer-based nanocarriers and a biomembrane for targeted drug delivery and gene therapy.<sup>32</sup> Owing to the development of advanced SSNMR methods, one can probe the complex internal nanostructure and heterogeneous dynamics of the NPs.

In this work, we present a new multiscale solid-state NMR approach for probing the internal morphology and nanostructure size, interfacial interaction, and dynamics of chitosan–poly(N-3-acrylamidophenylboronic acid) (CS-PAPBA) NPs. A recently developed <sup>13</sup>C multiple-CP/MAS method was first used to quantitatively determine the composition of the NPs and detect conformational changes in chitosan. Then, using an improved <sup>1</sup>H spin-diffusion technique with <sup>13</sup>C detection and theoretical simulations, the internal morphology and nanostructure size were quantitatively determined. The interfacial coordinated interaction between CS and phenylboronic acid of PAPBA was revealed by 1D MAS and two-dimensional triple-quantum MAS (2D 3QMAS) <sup>11</sup>B experiments. Furthermore,

dynamic-editing <sup>13</sup>C MAS and 2D <sup>13</sup>C–<sup>1</sup>H wide-line separation (WISE) experiments were utilized to determine the detailed componential dynamics of the NPs in the solid and swollen states. Finally, on the basis of these NMR results, a model for the unique nanostructure, interfacial interaction, and componential dynamics of the NPs was proposed. To the best of our knowledge, this is the first report to reveal the internal nanostructure and dynamics of chitosan-based nanoparticles.

## 2. MATERIALS AND METHODS

**2.1. Materials.** Chitosan with an average molecular weight ( $M_n$ ) of 5000 was purchased from Yuhuan Biomedical Company. The degree of deacetylation of chitosan was determined to be 83% using quantitative <sup>13</sup>C CPMAS NMR. 3-Acrylamidophenylboronic acid (APBA) was purchased from Frontier Scientific (FSI). K<sub>2</sub>S<sub>2</sub>O<sub>8</sub> was purchased from J&K Chemical. All analytical reagents were used as received.

**2.2. Preparation of Chitosan–Poly(N-3-acrylamidophenylboronic acid) Nanoparticles.** N-3-Acrylamidophenylboronic acid (APBA) was initially synthesized as in Zhang's previous work.<sup>33</sup> CS-PAPBA NPs were prepared through the radical polymerization of APBA in the presence of chitosan in aqueous medium.<sup>9</sup> The feed molar ratio of glucosamine units to APBA in the NPs was 1:1. First, 120 mg of APBA was dissolved in 10 mL of distilled water. Then, 100 mg of chitosan was added to the system after the solution became clear at 70 °C. When the chitosan dissolved completely, the system was cooled to room temperature, and the desired amount of K<sub>2</sub>S<sub>2</sub>O<sub>8</sub> as an initiator was added to the solution. After the system was adjusted to pH 5.0 with a sodium hydroxide solution and degassed, polymerization was initiated at 90 °C under a N<sub>2</sub> atmosphere for 2 h. The resultant solution was dialyzed against 1 L of distilled water for 24 h using a dialysis bag (MWCO 100 kDa). The dialyzed solution was then lyophilized at –50 °C. In addition, we obtained a hybrid sample of chitosan and APBA under the same conditions without polymerization; the sample was denoted NPs0.

**2.3. SEM and XRD Experiments.** SEM imaging was performed using a Shimadzu SS-550 SEM, with the samples dispersed in ethanol, drop-cast onto glass slips, and dried. X-ray diffraction (XRD) experiments were performed in reflection mode on a Rigaku D/max-2500 X-ray powder diffractometer with Cu KR ( $\lambda = 0.154$  nm) radiation at a generator voltage of 40 kV and a current of 100 mA.

**2.4. Solid-State NMR Experiments.** NMR experiments were performed on a Varian Infinityplus-400 wide-bore (89 mm) NMR spectrometer at room temperature (25 °C) and at frequencies of 399.72, 100.52, and 128.24 MHz for <sup>1</sup>H, <sup>13</sup>C, and <sup>11</sup>B, respectively. For the <sup>1</sup>H and <sup>13</sup>C experiments, a CP/MAS T3 probe with a rotor diameter of 4 mm was used, and samples with a volume of 52  $\mu$ L were placed in a zirconia PENCIL rotor. The MAS was automatically controlled with a speed controller for all 1D and 2D experiments. To obtain well-resolved <sup>13</sup>C NMR spectra, high-power <sup>1</sup>H-decoupling conditions via the SPINAL-64 technique<sup>34</sup> in a decoupling field of approximately 70 kHz and TOSS (total suppression of spinning sidebands)<sup>35</sup> were adopted during <sup>13</sup>C signal acquisition. The <sup>1</sup>H and <sup>13</sup>C chemical shifts were referenced to external TMS (0 ppm) and HMB (hexamethylbenzene, 17.3 ppm of CH<sub>3</sub>), respectively. The pulse sequences and detailed descriptions of the quantitative <sup>13</sup>C multiple-CP,<sup>28</sup> <sup>13</sup>C CPMAS, and DPMAS experiments,<sup>36,37</sup> in addition to the 2D <sup>13</sup>C–<sup>1</sup>H WISE<sup>20</sup> experiments, can be found in the literature. For all <sup>11</sup>B experiments, a CP/MAS T3 probe with a rotor diameter of 2.5 mm was used, and samples with a volume of 11  $\mu$ L were placed in a zirconia PENCIL rotor. The MAS was automatically controlled at 25 kHz, which sufficed to remove the spinning sidebands from the central portion of the spectrum. For the <sup>11</sup>B MAS NMR experiment, a single RF pulse (~0.2  $\mu$ s) corresponding to a ~20° flip angle was applied to obtain accurate <sup>11</sup>B intensities in various structural environments. The <sup>11</sup>B 2D multiple quantum (MQ) MAS spectrum (for  $I = \frac{3}{2}$ ) was obtained with a z-filtered split-t1 sequence,<sup>29</sup> in which fast amplitude modulated pulses were applied in the second pulse to achieve

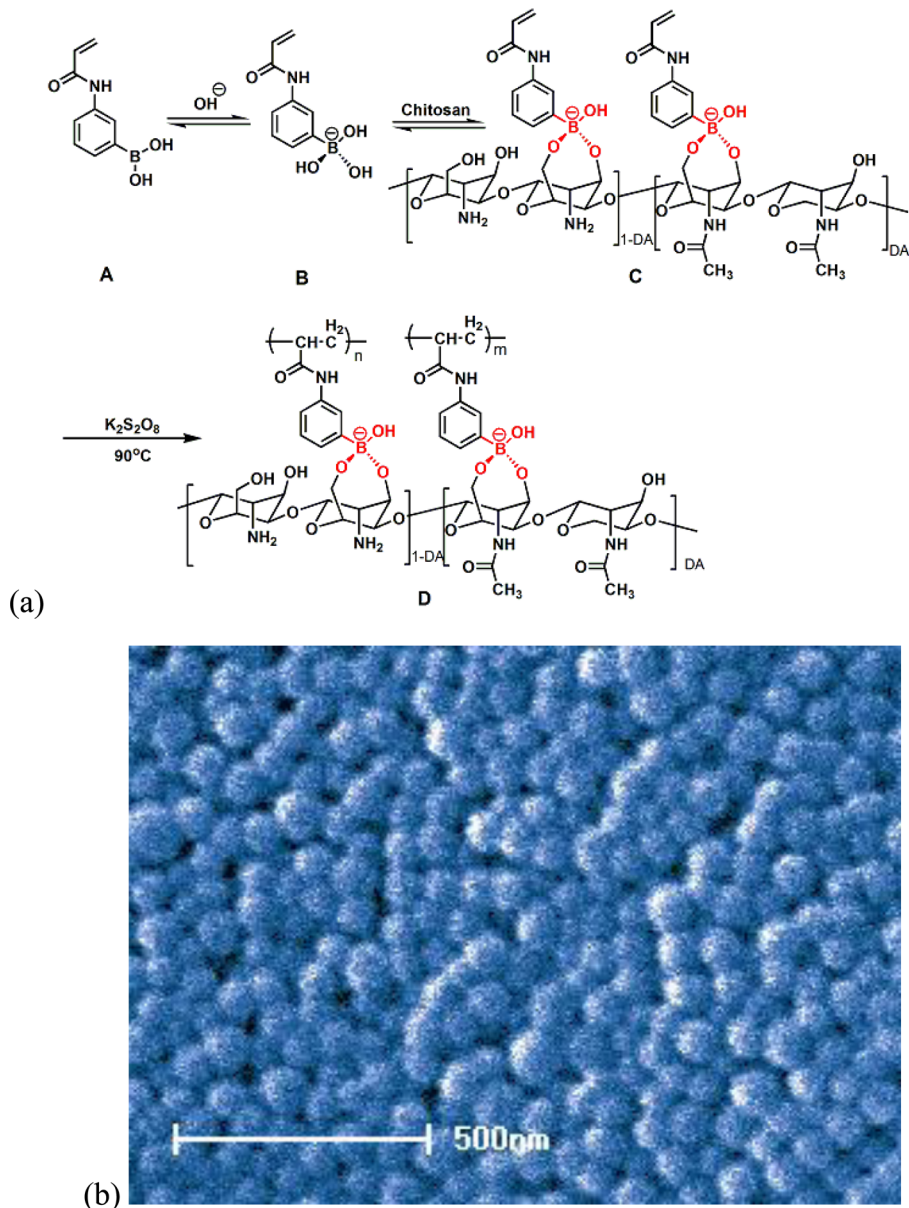


Figure 1. (a) Schematic diagram of the synthesis pathway of the CS-PAPBA NPs. (b) SEM micrograph of the NPs. The scale bar is 500 nm.

sensitivity enhancement.<sup>38</sup> The radio frequency power used was sufficient to produce a selective  $\pi/2$  pulse in 0.9  $\mu$ s for the spin- $3/2$  nuclei. The 6-phase cycling scheme used to simultaneously select 3Q coherence pathways was combined with classical CYCLOPS to eliminate receiver artifacts and with a States et al. scheme to produce pure-phase 2D spectra.<sup>39</sup> The 2D spectra are presented in the figures without shearing transformation. The <sup>11</sup>B chemical shift was referenced to that of a saturated boric acid aqueous solution at 19.5 ppm. The quadrupolar parameters and isotropic chemical shift were obtained directly from the 1D MAS spectra by using the simulation program DMFIT.<sup>40</sup>

**2.5. Simulation of <sup>1</sup>H Spin Diffusion.** The simulation of the <sup>1</sup>H spin-diffusion process from the source to the sink phase in a two-phase system was adapted from the work of Blümich et al.<sup>41</sup> The diffusion coefficient of the rigid phase, A, can be calculated from the following equation, which is valid for a Gaussian line shape<sup>42</sup>

$$D_A = \frac{1}{12} \sqrt{\frac{\pi}{2 \ln 2}} \left\langle r^2 \right\rangle \Delta\nu_{1/2}^A \quad (1)$$

where  $\Delta\nu_{1/2}^A$  is the line width of proton wide-line signals obtained by the results of 2D WISE experiments for rigid phase A.  $\langle r^2 \rangle$  is the mean-

square distance between the nearest spins (typically on the order of 0.04–0.06 nm<sup>2</sup>). The simulation program was written in the FORTAN language in our lab.

### 3. RESULTS AND DISCUSSION

**3.1. Determination of Composition and Conformational Changes by Quantitative <sup>13</sup>C CPMAS Experiments.** The synthesis pathway of CS-PAPBA NPs is summarized in Figure 1a.<sup>9</sup> The coordination and conformation of boron vary as the structural environment changes. APBA monomer is known to form a cyclic ester with saccharides such as chitosan in a specific pH environment. The boron site in hydrophobic APBA (Figure 1a-A) changes from the nonionic trigonal boronic form (B[3]) to the anionic tetrahedral boronate form (B[4]) (Figure 1a-B) by the coordination between APBA and OH<sup>-</sup>. Structure B in Figure 1a is favorable for combination with chitosan to form a stable and hydrophilic cyclic ester (Figure 1a-C). Then, APBA monomers are polymerized into PAPBA chains after being initiated by

$K_2S_2O_8$  (Figure 1a-D). Finally, the hydrophobic PAPBA and hydrophilic CS chains self-assemble into CS-PAPBA NPs. The morphology and particle size of the NPs was determined by SEM, as shown in Figure 1b. All of the formed NPs exhibited a spherical shape with a narrowly distributed diameter of approximately 80 nm. Because chitosan is hydrophilic, whereas PAPBA is hydrophobic, a particle with a PAPBA core and chitosan shell structure is generally expected. However, the commonly used TEM cannot provide any information regarding the inner nanostructure of the particles as reported on the same NPs,<sup>9</sup> which will be elucidated by multiscale SSNMR in the following section.

Quantification of composition is critical for the characterization of the NPs examined in this study. The obtained NPs formed a suspension in water; however, the molar ratio of the glucosamine unit to the APBA unit in the NPs cannot be determined by traditional solution  $^1H$  NMR because the NPs are insoluble in commonly used deuterated solvents or their mixtures thereof, such as DMSO/ $D_2O$ . High-resolution  $^{13}C$  CPMAS is a powerful method for investigating the microstructure and intermolecular interactions of organic solids because of its sensitivity to local chemical environments. However, the technique is still not a quantitative method because of the variation in CP efficiency among different carbons. Recently, a novel quantitative  $^{13}C$  CPMAS NMR technique using multiple CP was developed for probing organic materials, providing a new method for the quantitative determination of the composition of NPs.<sup>27</sup> Figure 2a shows the quantitative  $^{13}C$  CPMAS NMR spectra of NPs and pristine chitosan. On the basis of the integration of different peaks, the molar ratio of the glucosamine unit to the APBA unit in the NPs was easily determined to be 0.6:1, whereas the feed molar ratio was 1:1, which indicates that a small amount of CS is lost during the synthesis process. Determination of the NPs composition is important for the particles' applications. It has been observed that the proportion of chitosan in such NPs has a significant effect on controlling the pH response and the target drug delivery performance of the NPs.<sup>9</sup>

In addition to quantification of the composition, quantitative  $^{13}C$  CPMAS also provides critical information regarding microstructure and changes thereof. Figure 2a illustrates the remarkable change in the  $^{13}C$  CPMAS spectrum of chitosan in the NPs relative to the spectrum of pure chitosan. It is noteworthy that two C1 peaks at approximately 102 and 98 ppm can be observed in the NPs spectrum, whereas the spectrum of pure chitosan shows only a narrow C1 peak at approximately 98 ppm. In contrast, the overlapped C5 and C3 peaks in the NPs spectrum split into two peaks in the pure chitosan spectrum. These results indicate that a remarkable conformational change in chitosan should occur after the formation of NPs. To verify this conclusion, X-ray diffraction (XRD) experiments were performed to measure the crystallinity of the NPs, unreacted NPs (NPs0), and CS, the results of which are shown in Figure 2b. The figure shows that the sharp peaks of crystalline chitosan at  $6^\circ$  to  $12^\circ$  completely disappear in the NPs0 and NPs spectra. This result indicates that the incorporation of APBA significantly decreases the crystalline structure of chitosan. The sharp peaks ranging from  $25^\circ$  to  $46^\circ$  in the NPs0 spectrum are assigned to the crystalline APBA monomer. The conformational change of chitosan in the NPs, as indicated by XRD, is in good agreement with the findings of the  $^{13}C$  CPMAS experiments regarding the conformational change of chitosan in the NPs. Crystallization is known to be an

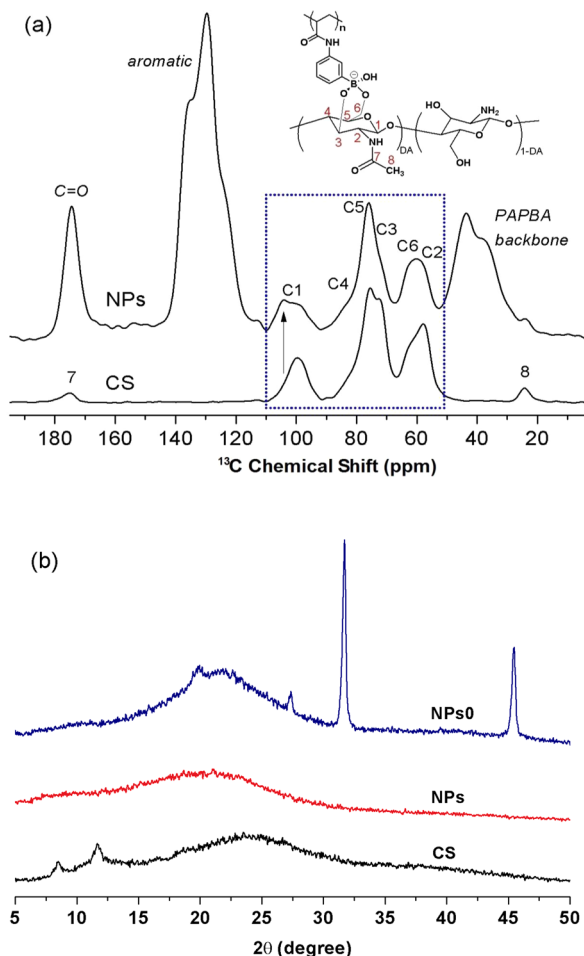


**Figure 2.** (a) Quantitative  $^{13}C$  CPMAS spectra of NPs and pristine chitosan. (b) XRD patterns of the chitosan, NPs, and NPs0.

important factor for the bioavailability of pharmaceuticals; indeed, high crystallization leads to poor bioavailability.<sup>9</sup> Figure 2a shows that incorporation of PAPBA increases the disorder of chitosan, indicating that boronic acid-rich chitosan NPs should exhibit better availability for drug delivery.

**3.2. Determination of the Internal Morphology and Domain Sizes of the NPs by  $^1H$  Spin-Diffusion Experiments with  $^{13}C$  Detection.** Determination of the inner morphology and domain sizes of CS-PAPBA NPs remains a great challenge because traditional methods such as SEM and TEM cannot provide such information. In contrast,  $^1H$  spin-diffusion experiments provide a powerful method for determining not only the morphology but also the domain sizes of nanostructured polymers at length scales ranging from the size of one monomer unit to 150 nm.<sup>19,41</sup> For multiphase polymers with distinct componential dynamics,  $^1H$  dipolar filter or double-quantum filter with  $^1H$  spin-diffusion has been widely used to determine domain sizes.<sup>43</sup> In contrast, for a multiphase polymer with two rigid components, the  $^1H$  chemical shift filter (CSF) is an effective method for creating a gradient of magnetization, which depends on the resolution of the  $^1H$  CRAMPS (combined rotation and multiple-pulse spectroscopy) spectrum.<sup>44,45</sup> Recent progress demonstrates that the morphology and domain sizes of heterogeneous polymers can also be determined by the theoretical simulation of spin-diffusion curves, even though the filter efficiency afforded by the above two types of techniques is not ideal.<sup>24</sup>

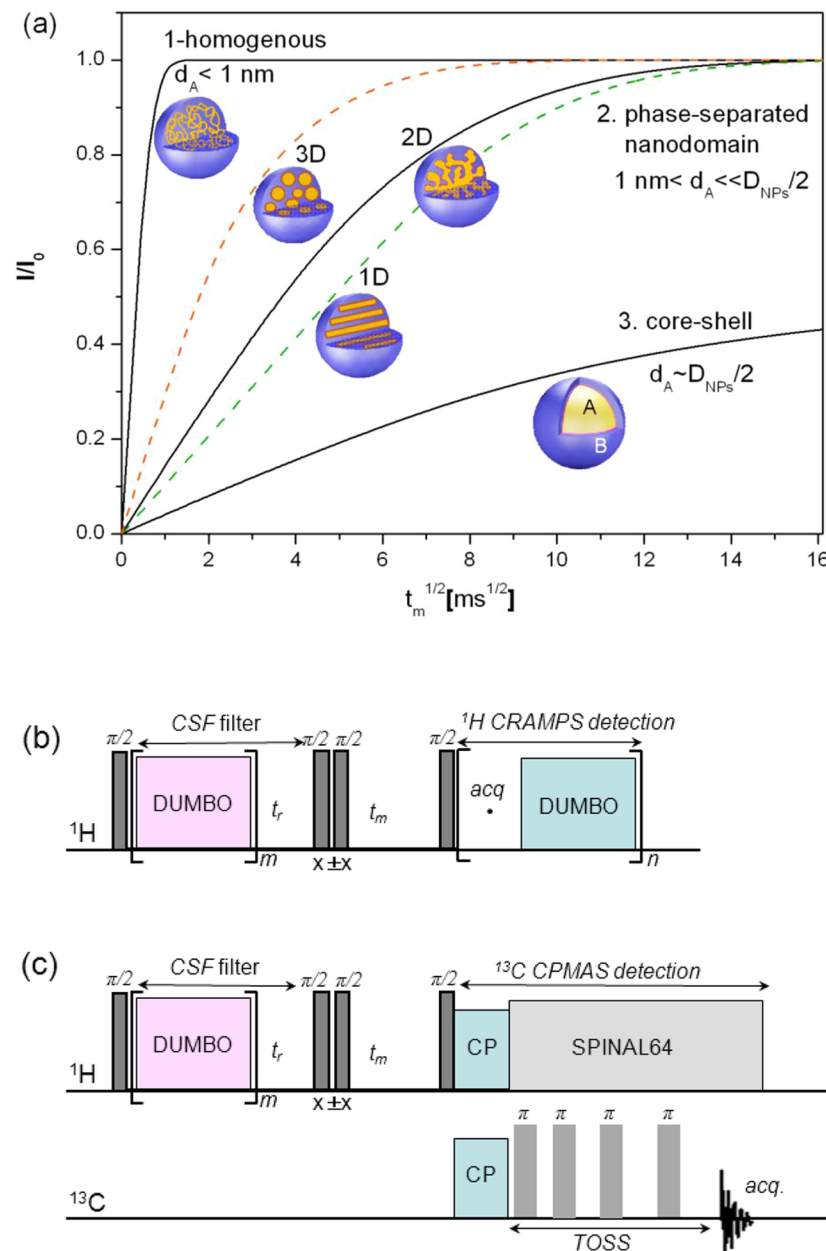


**Figure 3.** (a) Schematic diagram for determining different types of inner morphologies and domain sizes of polymer-based NPs from the simulation of  $^1\text{H}$  spin-diffusion buildup curves.  $D_{NPs}$  is the diameter of the NPs. 1D, 2D, and 3D curves correspond to phase separated NPs (type 2). (b, c)  $^1\text{H}$  CSF with spin-diffusion pulse sequences with (b)  $^1\text{H}$  CRAMPS or (c)  $^{13}\text{C}$  CPMAS detection.  $t_r$  and  $t_m$  are the time required for the transverse relaxation of undesired  $^1\text{H}$  magnetization and the mixing time, respectively. The phase cycling for the two  $90^\circ$  pulses before  $t_m$  is used to reduce the  $T_{1\text{H}}$  effect.<sup>44</sup>

Despite numerous advances, to the best of our knowledge, few NMR studies have reported the internal morphology and sizes of hybrid polymer-based NPs, especially those in which all components are rigid. Herein, we present a new solid-state NMR approach for determining the nanostructure of polymer-based NPs: The internal morphology and sizes of the NPs are determined from the theoretical simulation of  $^1\text{H}$  spin-diffusion buildup curves,<sup>24</sup> as shown in Figure 3a, which are measured by  $^1\text{H}$  spin-diffusion experiments with  $^1\text{H}$  or  $^{13}\text{C}$  detection depending on their resolution. If the determined domain size of the dispersed phase A,  $d_A$ , is smaller than 1 nm, then a homogeneous mixture should form inside the NPs (type 1 in Figure 3a). If  $d_A$  is close to the radius ( $D_{NPs}/2$ ) of the NPs, then

a core–shell structure should form (type 3 in Figure 3a). In other cases (type 2 in Figure 3a), a phase-separated nanostructure with 1D (lamellar), 2D (tubular), or 3D (spherical) morphologies should form.

Because both chitosan and PAPBA are rigid in the NPs (see 2D WISE experiment below), we utilized the  $^1\text{H}$  CSF method to measure the spin-diffusion curves of groups in one phase. To obtain a high-resolution  $^1\text{H}$  CSF spectrum and good experimental performance, we propose an improved  $^1\text{H}$  CSF pulse sequence with  $^1\text{H}$  or  $^{13}\text{C}$  detection, as shown in Figure 3b,c, which is based on the high-efficiency homonuclear decoupling using continue-phase-modulation (DUMBO) technique developed by Emsley et al.<sup>46,47</sup> The  $^1\text{H}$  CSF sequence is used to select the  $^1\text{H}$  magnetization of chemical groups in one

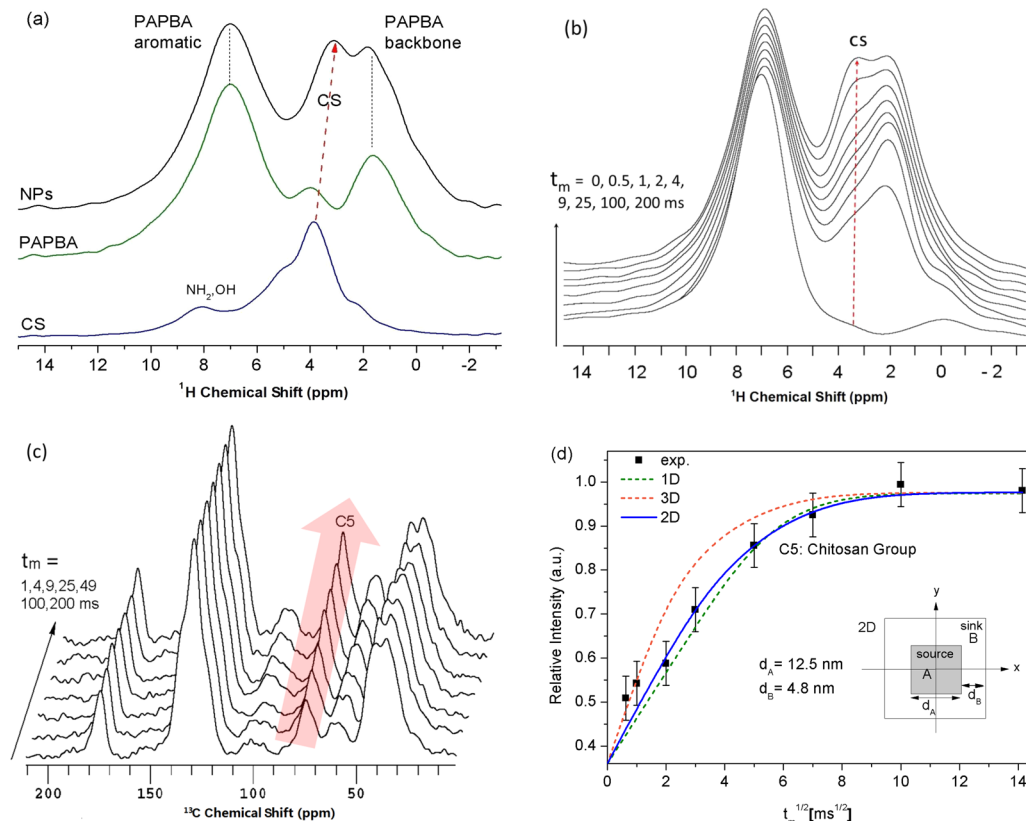


**Figure 4.** (a) <sup>1</sup>H CRAMPS spectra of NPs, PAPBA, and CS. (b) Chemical shift filter spectra of the NPs at different <sup>1</sup>H spin-diffusion times *t*<sub>m</sub> of 0, 0.5, 1, 4, 9, 25, 100, and 200 ms. (c) Stacked <sup>1</sup>H spin-diffusion spectra with <sup>13</sup>C CPMAS detection at different mixing times *t*<sub>m</sub>. (d) Time dependence of the <sup>13</sup>C-detected <sup>1</sup>H chemical shift-filtered spin-diffusion signal intensities of the chitosan C5 peak in the NPs; T<sub>1H</sub> correction of all data was adopted. All error bars are estimated as 75% of the peak-to-peak noise in the spectra. The lines are simulated spin-diffusion curves with different two-phase morphologies from 1D to 3D, and the solid line gives the best fit. Two-phase and 2D spin-diffusion models are also illustrated in the figure.

domain, which then spin-diffuses to another domain over period *t*<sub>m</sub> (mixing time). Compared with <sup>1</sup>H detection, <sup>13</sup>C detection usually provides better signal resolution for complex NPs; therefore, the <sup>1</sup>H magnetization is then transferred via CP to <sup>13</sup>C. To determine the domain sizes and morphology from the simulation, the spin-diffusion coefficient of the CS and PAPBA phases should be determined.

The average line widths of CS and PAPBA determined from slices of the WISE experiment on the NPs are 40 and 39 kHz, respectively; thus, the calculated diffusion coefficients of CS and PAPBA from eq 1 are 0.3 nm<sup>2</sup>/ms. The proton densities of the two components used in the simulation are set to 0.1 g/cm<sup>3</sup> (a typical value for polymers), with little effect on the spin-diffusion results.<sup>26</sup>

Figure 4a shows the DUMBO-based high-resolution <sup>1</sup>H CRAMPS<sup>48</sup> of chitosan PAPBA and the NPs. It is noted that the strong peak at 4 ppm for pristine chitosan shifts to 3.3 ppm for the NPs, indicating a change in the conformation of chitosan, which is in good agreement with the results from the <sup>13</sup>C CPMAS experiments shown in Figure 2a. Figure 4b shows the <sup>1</sup>H CSF spectra as a function of spin-diffusion mixing time (*t*<sub>m</sub>) from 0 to 200 ms. At *t*<sub>m</sub> = 0, all signals except the peaks at approximately 7 ppm are nearly completely suppressed; thus, a gradient in the magnetization is created. At *t*<sub>m</sub> > 0, we can observe a gradual increase in the suppressed CS signal at approximately 3.3 ppm with increasing *t*<sub>m</sub>, indicating the presence of <sup>1</sup>H spin diffusion among different groups. It should be noted that the signals of the CS and PAPBA groups still

overlap in the <sup>1</sup>H CSF spectra at *t*<sub>m</sub> > 0. Therefore, site-resolved <sup>13</sup>C detection in the <sup>1</sup>H CSF experiments is required to obtain the spin-diffusion buildup curves. However, the small NH<sub>2</sub> and OH signals of CS still overlap with the aromatic groups in PAPBA at *t*<sub>m</sub> = 0; it should be emphasized that recent work by Blümich et al. has proved that the <sup>1</sup>H spin-diffusion characteristic time is independent of the filter efficiency.<sup>24</sup> Thus, the residual NH<sub>2</sub> signal of CS at approximately 7 ppm does not affect the results regarding domain sizes. Figure 4c shows the <sup>13</sup>C-detected <sup>1</sup>H spin-diffusion spectra at *t*<sub>m</sub> = 1, 4, 9, 25, 49, 100, and 200 ms. Owing to the high resolution of the <sup>13</sup>C CPMAS spectra, we can quantitatively obtain the spin-diffusion curves of the chitosan signals (CS) as a function of the mixing time *t*<sub>m</sub>. Figure 4d shows the obtained spin-diffusion experimental data and the corresponding simulation results for different morphologies. It is noted that the initial signal of CS at *t*<sub>m</sub> = 0 is not zero because of the nonideal CSF filter for suppressing the chitosan signals, which does not affect the simulation results of the spin-diffusion curves. The 2D diffusion model used for the spin-diffusion simulations is also shown in this figure. It is interesting to note that a tubular (2D) inner morphology rather than the lamellar (1D) or commonly expected core–shell (3D) structure of the dispersed phase in the NPs gives the best fit to the spin-diffusion curves, and the obtained domain sizes of the PAPBA dispersed phase and CS are 12.5 and 4.8 nm, respectively, which are considerably smaller than the diameter (~80 nm) of the NPs. Because CS is

hydrophilic and PAPBA is hydrophobic, CS forms a continuous phase, whereas PAPBA forms a dispersed phase.

**3.3. Determination of the Interfacial Coordinated Interaction by  $^{11}\text{B}$  MAS and 3QMAS Experiments.** The interface between adjacent domains in NPs is an important factor in determining the final properties of a material. Intermolecular coordinate interactions between hydrophilic chitosan and the boronic acid group of hydrophobic PAPBA in the interface region are considered to be the driving force for the miscibility of the two components and the formation of the NPs. Therefore, the interactions have a crucial effect on the structure and properties of the NPs in practice.  $^{11}\text{B}$  MAS NMR has been frequently used to elucidate the types of coordination that occur in solid materials because of its sensitivity to local chemical environments.

Figure 5 shows the  $^{11}\text{B}$  MAS NMR spectra of NPs and unreacted NPs (NPs0) and their corresponding simulated

**Table 1. Parameters Obtained from  $^{11}\text{B}$  NMR Lineshape Simulation of the NPs and NPs0**

sample	$\delta$ iso (ppm)	$C_Q$ (MHz)	$\eta_Q$
NPs	$27.5 \pm 0.2$	$1.45 \pm 0.01$	$0.42 \pm 0.02$
NPs0	$27.8 \pm 0.2$	$1.50 \pm 0.01$	$0.42 \pm 0.02$

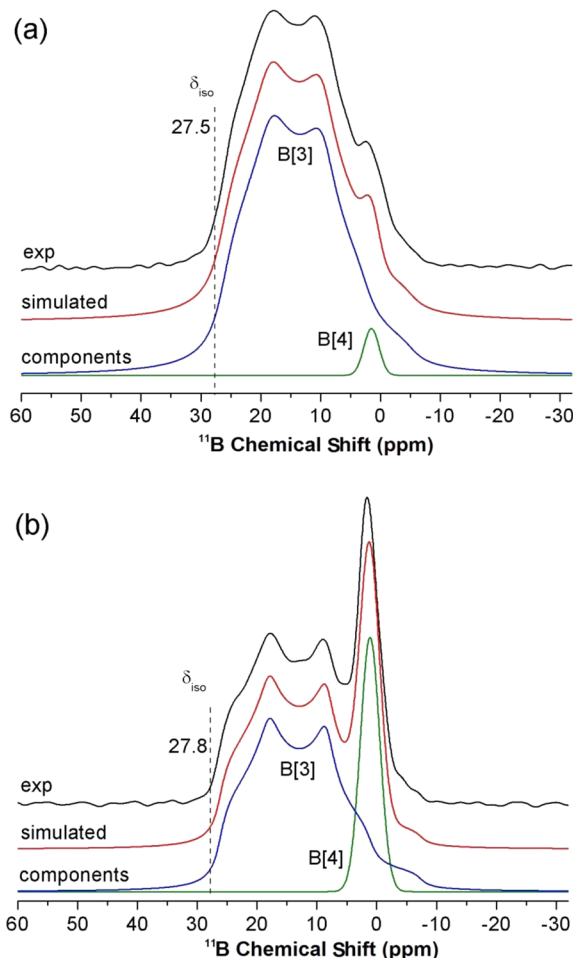


**Figure 5.**  $^{11}\text{B}$  MAS NMR experimental spectra (black line) and the corresponding simulated line shapes (red line) of (a) NPs and (b) NPs0.

quadrupole line shapes obtained from the DMFIT simulation program.<sup>39</sup> The calculated parameters of the B[3] components with large  $C_Q$  are listed in Table 1. Because  $^{11}\text{B}$  is a quadrupolar nucleus, both broad and narrow signals overlap in the MAS spectra, as shown in Figure 5. For the NPs, as shown in Figure 5a, a broad and strong peak caused by second-order quadrupolar interactions of boron in phenylboronic acid can be obtained, implying that most of the boron in the NPs is

present in the trigonal form, B[3]. In previous  $^{11}\text{B}$  NMR studies, only B[3] was observed for pure PAPBA powder; thus, the B[3] signal shown in Figure 5a should be assigned to the PAPBA in the NPs. The weak peak at 2.3 ppm shown in Figure 5a indicates the existence of four-coordinate boron B[4] in the NPs. Because the NPs contain 80% unmodified chitosan OH groups, the hydroxyl group of CS can coordinate with phenylboronic acid and trigger some boron to change from a trigonal planar configuration to a tetrahedral configuration. Therefore, the B[4] observed in Figure 5a should be assigned to the coordinate interaction between CS and PAPBA in the NPs. For NPs0, as shown in Figure 5b, both a broad B[3] signal and a sharp B[4] signal at approximately 1.6 ppm were observed. It is noteworthy that the B[4] signal was much stronger in NPs0 than in the NPs, indicating that the polymerization of APBA induced a decrease in the coordinate interaction between CS and PAPBA. Another reason is that the NPs sample was submitted to dialysis for several hours after polymerization; thus, residual B[4] monomers should have been eliminated. The strong B[3] signal in NPs0 also indicates that the majority of boron is still three-coordinate with PAPBA. It is also noted that the line shapes of NPs and NPs0 are clearly different, and the calculated quadrupole coupling constant  $C_Q$  of B[3] units in the NPs is smaller than that of the B[3] units in the NPs0, indicating the changes in the boron structural environment after polymerization. In addition to the phase separation, based on the integration intensity of the simulated line shapes of B[3] and B[4] shown in Figure 4, the content of B[4] was calculated to be approximately 3 and 22% in NPs and NPs0, respectively.

To better characterize the significantly overlapped B[3] and B[4] sites in the 1D  $^{11}\text{B}$  MAS NMR spectra of the NPs and NPs0, high-resolution 2D  $^{11}\text{B}$  3QMAS NMR experiments were further performed, through which different types of boron could be clearly distinguished in the F1 dimension without quadrupolar broadening. Figure 6 shows the 2D  $^{11}\text{B}$  3QMAS NMR spectrum of the NPs and NPs0. Separation of two different types of boron sites in these two samples is clearly observed. In the F2 dimension, the projection spectrum is superimposed by a weak B[4] signal and a strong signal covering the chemical shift from 0 to 30 ppm, with a typical second-order quadrupolar pattern arising from B[3] sites, as reported by Pruski et al.<sup>49</sup> In contrast, in the F1 dimension, these signals can be clearly resolved. Referring to Chen,<sup>50</sup> the signal at 2.5 ppm can be assigned to four-coordinate boron B[4] species, and the strong signal with large quadrupolar broadening is assigned to three-coordinate boron B[3] species. It is also noted that the peak intensity of B[4] signal is much weaker than that of B[3]. Because the molar ratio of glucosamine units to APBA in the NPs determined by quantitative  $^{13}\text{C}$  CPMAS NMR was 0.6:1, the observed weak B[4] species in the NPs associated with the coordinate interaction between CS and PAPBA implies that these two components are only partially miscible; thus, phase separation in the NPs should be expected. This result further confirms that

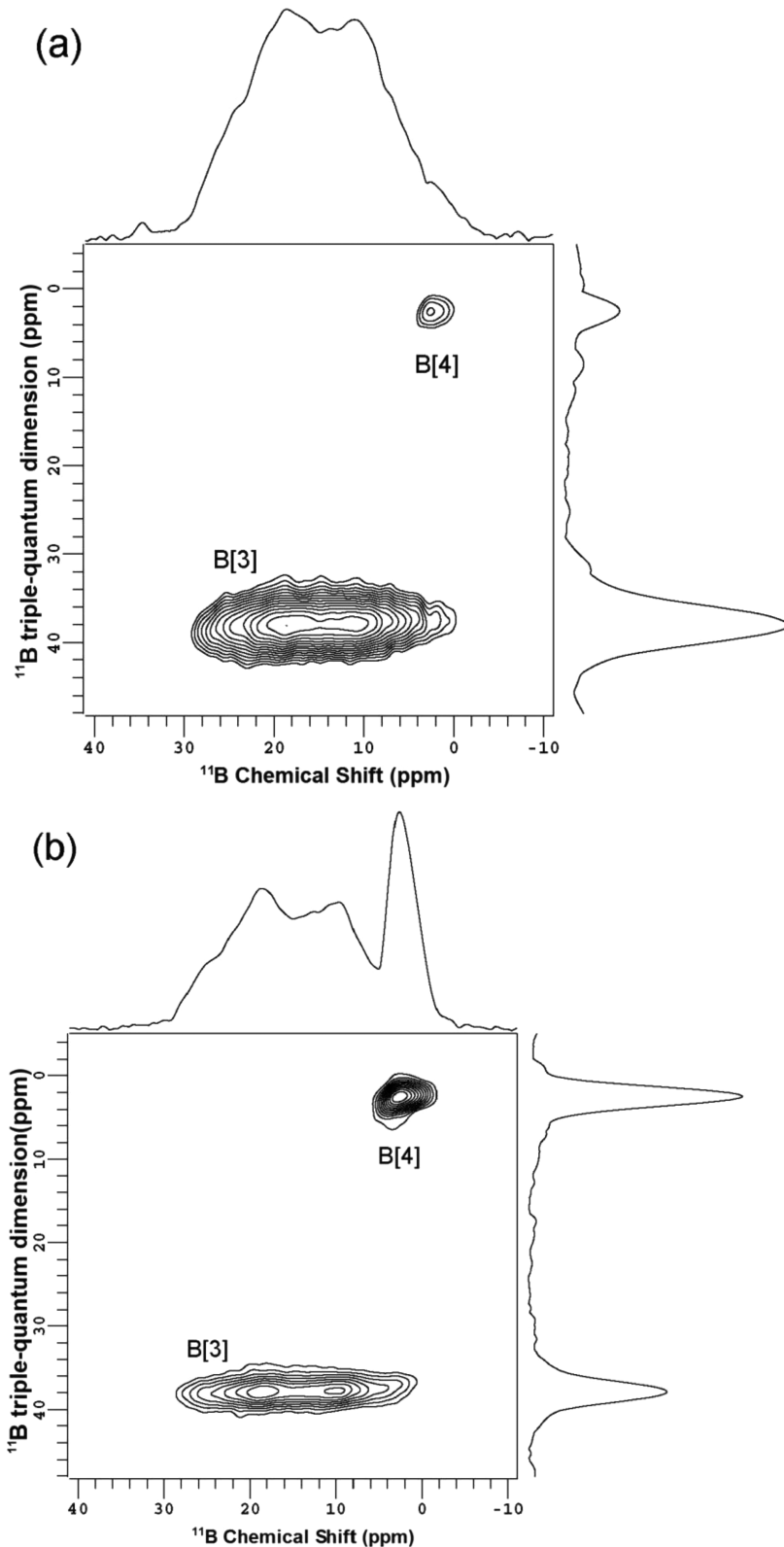


**Figure 6.**  $^{11}\text{B}$  3QMAS NMR spectra of (a) NPs and (b) NPs0.

phase separation occurs, as indicated by the foregoing  $^1\text{H}$  spin-diffusion NMR experiments.

**3.4. Componential Dynamics Determined by Dynamic Editing  $^{13}\text{C}$  and 2D  $^{13}\text{C}$ – $^1\text{H}$  WISE Experiments.** Componential dynamics are ubiquitous and exert important effects on the stability of pharmaceuticals<sup>51</sup> and the drug

delivery efficiency of NPs. For example, the stability of amorphous pharmaceuticals against crystallization is quite important in enhancing the particles' bioavailability in the pharmaceutical industry.<sup>9</sup> Moreover, segmental dynamics are quite important for controlling the diffusion efficiency of drugs enclosed in NPs. A computer model was recently developed to

simultaneously capture the diffusion of encapsulated drugs and the dynamics of the polymer chains of polymer-based NPs.<sup>15</sup> Therefore, a deep understanding of the componential dynamics that occur in NPs is also in high demand. 2D  $^{13}\text{C}$ – $^1\text{H}$  WISE experiments are widely used to characterize polymers with heterogeneous dynamics and multiphase structures that feature hard and soft components.<sup>19</sup> The components are distinguished by the  $^1\text{H}$  wide-line spectrum (F1 dimension); broad signals indicate rigid components, and narrow signals indicate mobile components. In contrast, the corresponding  $^{13}\text{C}$  chemical shifts in the F2 dimension indicate the chemical composition. Figure 7a shows the contour plot of the  $^{13}\text{C}$ – $^1\text{H}$  WISE spectrum of

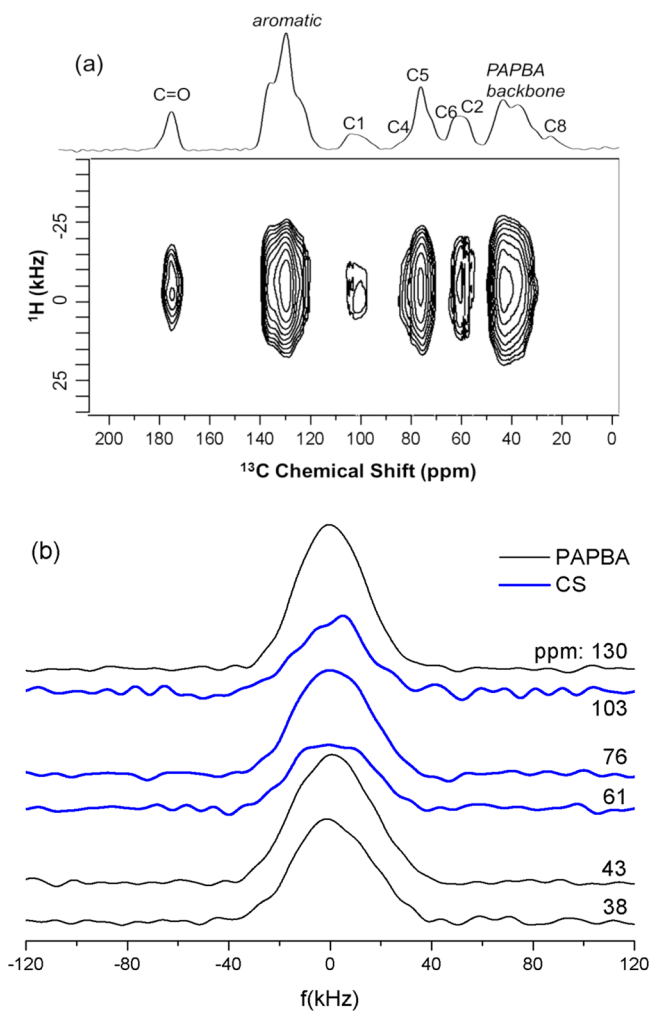


**Figure 7.** (a) 2D  $^{13}\text{C}$ – $^1\text{H}$  WISE contour spectrum of NPs. The  $^{13}\text{C}$  CPMAS spectrum of the NPs is also shown on top of the figure. (b) Slices of the 2D WISE spectrum at different carbon sites, in which the corresponding  $^{13}\text{C}$  chemical shifts (ppm) are indicated.

the NPs, and Figure 7b shows slices of the WISE spectrum at different carbon sites. It is noteworthy that the line shapes for all of the carbon sites are nearly Gaussian and the line half-widths are approximately 40 kHz, indicating that both PAPBA and chitosan in the NPs are very rigid in the solid state. In the swollen state, the mobile component could hardly be detected in the 2D WISE experiments because of the component's lower  $^1\text{H}$  to  $^{13}\text{C}$  CP efficiency. Instead, we used dynamic-editing  $^{13}\text{C}$  NMR methods to detect the componential dynamics in the NPs.  $^{13}\text{C}$  DPMAS with a short recycle delay is an efficient

method for detecting the mobile component.<sup>52</sup> Figure 8a shows the  $^{13}\text{C}$  DPMAS spectrum of the NPs swollen in  $\text{D}_2\text{O}$  with a

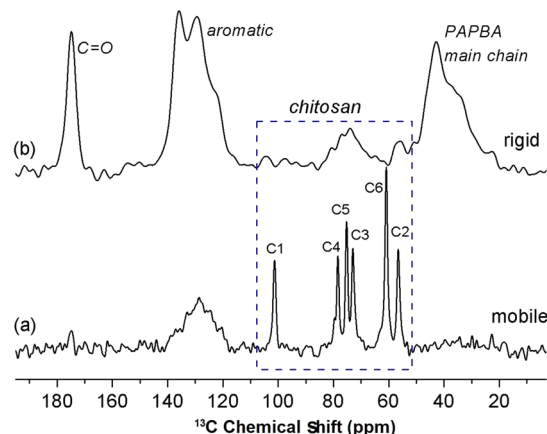


**Figure 8.**  $^{13}\text{C}$  NMR spectra of NPs swollen in  $\text{D}_2\text{O}$ : (a) mobile components detected by  $^{13}\text{C}$  DPMAS with short (0.3 s) recycle delay and (b) rigid components detected by the  $T_{1\text{C}}$ -filtered  $^{13}\text{C}$  CPMAS with a 6 s delay time.

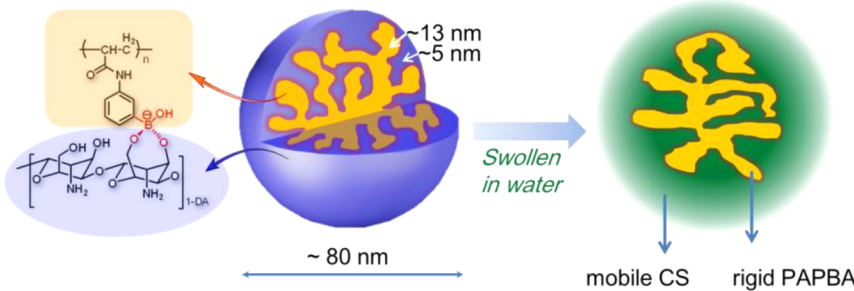
0.3 s short recycle delay. Strong signals for chitosan with well-resolved C1–C6 peaks were detected, indicating that the hydrophilic chitosan chains are extremely mobile and should reasonably give rise to a continuous phase. In contrast, only a weak signal from PAPBA was detected in the  $^{13}\text{C}$  direct-polarization MAS (DPMAS) spectrum, indicating that a small amount of PAPBA chains should intimately mix with chitosan in the interface region and can easily contact with water; thus, most of the rigid hydrophobic PAPBA forms a dispersed phase. Figure 8b shows the  $T_{1\text{C}}$ -filtered  $^{13}\text{C}$  CPMAS spectrum of the NPs swollen in  $\text{D}_2\text{O}$ , which shows only the rigid components exhibiting longer  $T_{1\text{C}}$ .<sup>35,36</sup> The presence of strong PAPBA signals in the dispersed phase indicates that most of the hydrophobic PAPBA chains are rigid.

**3.5. Suggested Model of the Nanostructure and Dynamics of the NPs.** On the basis of the SSNMR results discussed above, a comprehensive understanding of the internal morphology and sizes of the nanostructure, interfacial interaction, and componential dynamics of CS–PAPBA NPs can be achieved, and the model shown in Scheme 1 is proposed. The obtained supramolecular-assembled NPs exhibit a tubular internal morphology rather than the expected core–shell structure, in which the hydrophilic CS forms the continuous phase and hydrophobic PAPBA forms the tubular dispersed phase. The determined domain sizes of the PAPBA and CS phases are 12.5 and 4.8 nm, respectively. At the interphase between the two phases, a small amount of PAPBA intimately mixes with chitosan by means of the intermolecular four-coordinate boronic interaction. The incorporation of phenylboronic acid causes the conformation of CS to become disordered. Both components in the NPs are rigid in the solid state, whereas the chitosan segments become remarkably mobile when swollen in water.

#### 4. CONCLUSIONS

In this work, multiscale and multinuclear SSNMR techniques were used to successfully probe the internal morphology and nanostructure size, interfacial interaction, and dynamics of CS–PAPBA NPs. Quantitative  $^{13}\text{C}$  CPMAS experiments provided

**Scheme 1. Schematic Presentation of the Inner Morphology of the Nanostructure and Componential Dynamics of CS-PAPBA NPs in the Solid and Swollen States in Water**



fast quantification of the NPs' composition, which indicated that the proportion of CS decreased after sample preparation. The conformation of chitosan was observed to be disordered after incorporation with phenylboronic acid. Using improved  $^1\text{H}$  spin-diffusion methodology with  $^{13}\text{C}$  detection and theoretical simulations, a tubular internal morphology was detected in which the domain sizes of the hydrophilic continuous phase of CS and hydrophobic dispersed phase of PAPBA in the NPs were determined to be 12.5 and 4.8 nm, respectively.  $^{11}\text{B}$  1D MAS and 2D 3QMAS experiments revealed that only a small amount of CS segments interact with PAPBA segments through the B[4] coordinate interaction in the interfacial region, indicating that the two components are only partially miscible and further confirming the phase separation in the NPs. Finally, dynamic-editing NMR experiments indicated that chitosan chains are rigid in the solid state and mobile when swollen in water, whereas PAPBA chains are rigid in any state. On the basis of these NMR results, a model of the unique nanostructure, interfacial interaction, and componential dynamics of the NPs is proposed. This study demonstrates that solid-state NMR is intrinsically a powerful multiscale and versatile tool for revealing the internal nanostructure, composition, interface, and componential dynamics of polymer-based NPs that can promote the precise design and efficient biological application of these important and promising NPs.

## AUTHOR INFORMATION

### Corresponding Author

\*E-mail: spclbh@nankai.edu.cn.

### Notes

The authors declare no competing financial interest.

## ACKNOWLEDGMENTS

This work was supported by the National Science Fund for Distinguished Young Scholars (20825416), the National Natural Science Foundation of China (21374051), 973 program (2012CB821503), PCSIRT (IRT1257), CERS-1-61, and the 111 Project (B12015).

## REFERENCES

- (1) Verma, M. S.; Liu, S.; Chen, Y. Y.; Meerasa, A.; Gu, F. X. Size-Tunable Nanoparticles Composed of Dextran-B-Poly(D,L-lactide) for Drug Delivery Applications. *Nano Res.* **2012**, *5*, 49–61.
- (2) Guo, P.; Martin, C. R.; Zhao, Y.; Ge, J.; Zare, R. N. General Method for Producing Organic Nanoparticles Using Nanoporous Membranes. *Nano Lett.* **2010**, *10*, 2202–2206.
- (3) Mittnacht, U.; Hartmann, H.; Hein, S.; Oliveira, H.; Dong, M.; Pêgo, A.; Kjems, J.; Howard, K. A.; Schlosshauer, B. Chitosan/siRNA Nanoparticles Biofunctionalize Nerve Implants and Enable Neurite Outgrowth. *Nano Lett.* **2010**, *10*, 3933–3939.
- (4) Anitha, A.; Chennazhi, K. P.; Nair, S. V.; Jayakumar, R. 5-Flourouracil Loaded N,O-Carboxymethyl Chitosan Nanoparticles as an Anticancer Nanomedicine for Breast Cancer. *J. Biomed. Nanotechnol.* **2012**, *8*, 29–42.
- (5) Majedi, F. S.; Hasani-Sadrabadi, M. M.; VanDersarl, J. J.; Mokarram, N.; Hojjati-Emami, S.; Dashtimoghadam, E.; Bonakdar, S.; Shokrgozar, M. A.; Bertsch, A.; Renaud, P. On-Chip Fabrication of Paclitaxel-Loaded Chitosan Nanoparticles for Cancer Therapeutics. *Adv. Funct. Mater.* **2014**, *24*, 432–441.
- (6) Wei, P.-R.; Cheng, S.-H.; Liao, W.-N.; Kao, K.-C.; Weng, C.-F.; Lee, C.-H. Synthesis of Chitosan-Coated Near-Infrared Layered Double Hydroxide Nanoparticles for In Vivo Optical Imaging. *J. Mater. Chem.* **2012**, *22*, 5503–5513.
- (7) Dragan, E. S.; Mihai, M.; Schwarz, S. Complex Nanoparticles Based on Chitosan and Ionic/Nonionic Strong Polyanions: Formation, Stability, and Application. *ACS Appl. Mater. Interfaces* **2009**, *1*, 1231–1240.
- (8) Wang, B.; Ma, R.; Liu, G.; Liu, X.; Gao, Y.; Shen, J.; An, Y.; Shi, L. Effect of Coordination on the Glucose-Responsiveness of PEG-B-(PAA-co-PAAPBA) Micelles. *Macromol. Rapid Commun.* **2010**, *31*, 1628–1634.
- (9) Wang, X.; Zhen, X.; Wang, J.; Zhang, J.; Wu, W.; Jiang, X. Doxorubicin Delivery to 3D Multicellular Spheroids and Tumors Based on Boronic Acid-Rich Chitosan Nanoparticles. *Biomaterials* **2013**, *34*, 4667–4679.
- (10) Hu, Y.; Jiang, X. Q.; Ding, Y.; Ge, H. X.; Yuan, Y. Y.; Yang, C. Z. Synthesis and Characterization of Chitosan-Poly(acrylic acid) Nanoparticles. *Biomaterials* **2002**, *23*, 3193–3201.
- (11) Xu, G.-K.; Feng, X.-Q.; Yu, S.-W. Controllable Nanostructural Transitions in Grafted Nanoparticle-Block Copolymer Composites. *Nano Res.* **2010**, *3*, 356–362.
- (12) Salam, A.; Lucia, L. A.; Jameel, H. Synthesis, Characterization, and Evaluation of Chitosan-Complexed Starch Nanoparticles on the Physical Properties of Recycled Paper Furnish. *ACS Appl. Mater. Interfaces* **2013**, *5*, 11029–11037.
- (13) Yoo, S. I.; Yang, M.; Brender, J. R.; Subramanian, V.; Sun, K.; Joo, N. E.; Jeong, S. H.; Ramamoorthy, A.; Kotov, N. A. Inhibition of Amyloid Peptide Fibrillation by Inorganic Nanoparticles: Functional Similarities with Proteins. *Angew. Chem., Int. Ed.* **2011**, *50*, 5110–5115.
- (14) Yue, Z.-G.; Wei, W.; Lv, P.-P.; Yue, H.; Wang, L.-Y.; Su, Z.-G.; Ma, G.-H. Surface Charge Affects Cellular Uptake and Intracellular Trafficking of Chitosan-Based Nanoparticles. *Biomacromolecules* **2011**, *12*, 2440–2446.
- (15) He, N.-P.; Du, X.; Huang, S.-K. Preparation of Chitosan-Poly(acrylic acid) Nanoparticles and Its Solubilizing Abilities for Water-Insoluble Drugs. *J. Controlled Release* **2013**, *172*, E58–E59.
- (16) Durbin, E. W.; Buxton, G. A. A Coarse-Grained Model of Targeted Drug Delivery from Responsive Polymer Nanoparticles. *Soft Matter* **2010**, *6*, 762–767.
- (17) Zeng, L.; Alemany, L. B.; Edwards, C. L.; Barron, A. R. Demonstration of Covalent Sidewall Functionalization of Single Wall Carbon Nanotubes by NMR Spectroscopy: Side Chain Length

- Dependence on the Observation of the Sidewall Sp<sup>3</sup> Carbons. *Nano Res.* **2008**, *1*, 72–88.
- (18) Marega, R.; Aroulmoji, V.; Bergamin, M.; Feruglio, L.; Dinon, F.; Bianco, A.; Murano, E.; Prato, M. Two-Dimensional Diffusion-Ordered NMR Spectroscopy as a Tool for Monitoring Functionalized Carbon Nanotube Purification and Composition. *ACS Nano* **2010**, *4*, 2051–2058.
- (19) Qian, H.; Zhu, M.; Gayathri, C.; Gil, R. R.; Jin, R. Chirality in Gold Nanoclusters Probed by NMR Spectroscopy. *ACS Nano* **2011**, *5*, 8935–8942.
- (20) Schmidt-Rohr, S. H. *Multiple Dimensional NMR and Polymers*; Academic Press: San Diego, CA, 1994.
- (21) Wilhelm, M.; Feng, H.; Tracht, U.; Spiess, H. W. 2D CP/MAS <sup>13</sup>C Isotropic Chemical Shift Correlation Established by <sup>1</sup>H Spin Diffusion. *J. Magn. Reson.* **1998**, *134*, 255–260.
- (22) Pena, B.; de Menorval, L.-C.; Garcia-Valls, R.; Gumi, T. Characterization of Polysulfone and Polysulfone/Vanillin Microcapsules by <sup>1</sup>H NMR Spectroscopy, Solid-State <sup>13</sup>C CP/MAS-NMR Spectroscopy, and N<sub>2</sub> Adsorption Desorption Analyses. *ACS Appl. Mater. Interfaces* **2011**, *3*, 4420–4430.
- (23) Fortier-McGill, B.; Toader, V.; Reven, L. <sup>13</sup>C MAS NMR Study of Poly(methacrylic acid)-Polyether Complexes and Multilayers. *Macromolecules* **2014**, *47*, 4298–4307.
- (24) Fortier-McGill, B.; Toader, V.; Reven, L. <sup>1</sup>H Solid State NMR Study of Poly(methacrylic acid) Hydrogen-Bonded Complexes. *Macromolecules* **2012**, *45*, 6015–6026.
- (25) Buda, A.; Demco, D. E.; Bertmer, M.; Blumich, B.; Reining, B.; Keul, H.; Hocker, H. Domain Sizes in Heterogeneous Polymers by Spin Diffusion Using Single-Quantum and Double-Quantum Dipolar Filters. *Solid State Nucl. Magn. Reson.* **2003**, *24*, 39–67.
- (26) Katharina Landfester, C. B.; Morand, L.; Spiess, H. W. Characterization of Interfaces in Core-Shell Polymers by Advanced Solid-State NMR Methods. *Macromolecules* **1996**, *29*, 5972–5980.
- (27) Kumashiro, K. K.; Schmidt-Rohr, K.; Murphy, O. J.; Ouellette, K. L.; Cramer, W. A.; Thompson, L. K. A Novel Tool for Probing Membrane Protein Structure: Solid-State NMR with Proton Spin Diffusion and X-Nucleus Detection. *J. Am. Chem. Soc.* **1998**, *120*, 5043–5051.
- (28) Johnson, R. L.; Schmidt-Rohr, K. Quantitative Solid-State <sup>13</sup>C NMR with Signal Enhancement by Multiple Cross Polarization. *J. Magn. Reson.* **2014**, *239*, 44–49.
- (29) Brown, S. P.; Wimperis, S. Two-Dimensional Multiple-Quantum MAS NMR of Quadrupolar Nuclei: A Comparison of Methods. *J. Magn. Reson.* **1997**, *128*, 42–61.
- (30) Madhu, P. K.; Goldbourt, A.; Frydman, L.; Vega, S. Fast Radio-Frequency Amplitude Modulation in Multiple-Quantum Magic-Angle-Spinning Nuclear Magnetic Resonance: Theory and Experiments. *J. Chem. Phys.* **2000**, *112*, 2377–2391.
- (31) Io, T.; Fukami, T.; Yamamoto, K.; Suzuki, T.; Xu, J. D.; Tomono, K.; Ramamoorthy, A. Homogeneous Nanoparticles to Enhance the Efficiency of a Hydrophobic Drug, Antihyperlipidemic Probucol, Characterized by Solid-State NMR. *Mol. Pharmaceutics* **2010**, *7*, 299–305.
- (32) Smith, P. E. S.; Brender, J. R.; Dürr, U. H. N.; Xu, J.; Mullen, D. G.; Banaszak Holl, M. M.; Ramamoorthy, A. Solid-State NMR Reveals the Hydrophobic-Core Location of Poly(amidoamine) Dendrimers in Biomembranes. *J. Am. Chem. Soc.* **2010**, *132*, 8087.
- (33) Zhang, L. Z.; Lin, Y.; Wang, J. J.; Yao, W.; Wu, W.; Jiang, X. Q. A Facile Strategy for Constructing Boron-Rich Polymer Nanoparticles via a Boronic Acid-Related Reaction. *Macromol. Rapid Commun.* **2011**, *32*, 534–539.
- (34) Fung, B. M.; Khitrin, A. K.; Ermolaev, K. An Improved Broadband Decoupling Sequence for Liquid Crystals and Solids. *J. Magn. Reson.* **2000**, *142*, 97–101.
- (35) Hagemeyer, A.; Van Der Putten, D.; Spiess, H. W. The Use of Composite Pulse in the TOSS Experiment. *J. Magn. Reson.* **1991**, *92*, 628–630.
- (36) Mowery, D. M.; Harris, D. J.; Schmidt-Rohr, K. Characterization of a Major Fraction of Disordered All-Trans Chains in Cold-Drawn High-Density Polyethylene by Solid-State NMR. *Macromolecules* **2006**, *39*, 2856–2865.
- (37) Rongchun, Z.; Chen, Y. Z.; Chen, T. H.; Sun, P. C.; Li, B. H.; Ding, D. T. Accessing Structure and Dynamics of Mobile Phase in Organic Solids by Real-Time T<sub>1c</sub> Filter PISEMA NMR Spectroscopy. *J. Phys. Chem. A* **2012**, *116*, 979–984.
- (38) Goldbourt, A.; Kababya, S.; Vega, S.; Madhu, P. K. The Influence of the Radio-Frequency Excitation and Conversion Pulses on the Lineshapes and Intensities of the Triple-Quantum MAS NMR Spectra of I = 3/2 Nuclei. *Solid State Nucl. Magn. Reson.* **2000**, *18*, 1–16.
- (39) States, D. J.; Haberkorn, R. A.; Ruben, D. J. A Two-Dimensional Nuclear Overhauser Experiment with Pure Absorption Phase in Four Quadrants. *J. Magn. Reson.* **1982**, *48*, 286.
- (40) Massiot, D.; Fayon, F.; Capron, M.; King, I.; Le Calvé, S.; Alonso, B.; Durand, J.-O.; Bujoli, B.; Gan, Z.; Hoatson, G. Modelling One- and Two-Dimensional Solid-State NMR Spectra. *Magn. Reson. Chem.* **2002**, *40*, 70–76.
- (41) Voda, M. A.; Demco, D. E.; Voda, A.; Schaeber, T.; Adler, M.; Dabisch, T.; Adams, A.; Baias, M.; Blümich, B. Morphology of Thermoplastic Polyurethanes by <sup>1</sup>H Spin-Diffusion NMR. *Macromolecules* **2006**, *39*, 4802–4810.
- (42) Sun, P. C.; Dang, Q. Q.; Li, B. H.; Chen, T. H.; Wang, Y. N.; Lin, H.; Jin, Q. H.; Ding, D. T.; Shi, A. C. Mobility, Miscibility, and Microdomain Structure in Nanostructured Thermoset Blends of Epoxy Resin and Amphiphilic Poly(ethylene oxide)-Block-Poly(propylene oxide)-Block-Poly(ethylene oxide) Triblock Copolymers Characterized by Solid-State NMR. *Macromolecules* **2005**, *38*, 5654–5667.
- (43) Hedesiu, C.; Demco, D. E.; Kleppinger, R.; Buda, A. A.; Blümich, B.; Remerie, K.; Litvinov, V. M. The Effect of Temperature and Annealing on the Phase Composition, Molecular Mobility and the Thickness of Domains in High-Density Polyethylene. *Polymer* **2007**, *48*, 763–777.
- (44) Clauss, J.; Schmidt-Rohr, K.; Spiess, H. W. Determination of Domain Sizes in Heterogeneous Polymers by Solid-State NMR. *Acta Polym.* **1993**, *44*, 1.
- (45) VanderHart, D. L.; Prabhu, V. M.; Lin, E. K. Proton NMR Determination of Miscibility in a Bulk Model Photoresist System: Poly(4-hydroxystyrene) and the Photoacid Generator, Di(tert-butylphenyl)iodonium Perfluoroctanesulfonate. *Chem. Mater.* **2004**, *16*, 3074–3084.
- (46) Sakellarou, D.; Lesage, A.; Hodgkinson, P.; Emsley, L. Homonuclear Dipolar Decoupling in Solid-State NMR Using Continuous Phase Modulation. *Chem. Phys. Lett.* **2000**, *319*, 253–260.
- (47) Brown, S. P.; Lesage, A.; Elena, B.; Emsley, L. Probing Proton-Proton Proximities in the Solid State: High-Resolution Two-Dimensional <sup>1</sup>H–<sup>1</sup>H Double-Quantum CRAMPS NMR Spectroscopy. *J. Am. Chem. Soc.* **2004**, *126*, 13230–13231.
- (48) Li, B.; Xu, L.; Wu, Q.; Chen, T.; Sun, P.; Jin, Q.; Ding, D.; Wang, X.; Xue, G.; Shi, A. C. Various Types of Hydrogen Bonds, Their Temperature Dependence and Water–Polymer Interaction in Hydrated Poly(acrylic acid) as Revealed by <sup>1</sup>H Solid-State NMR Spectroscopy. *Macromolecules* **2007**, *40*, 5776–5786.
- (49) Hwang, S. J.; Fernandez, C.; Amoureux, J. P.; Han, J. W.; Cho, J.; Martin, S. W.; Pruski, M. Structural Study of xNa<sub>2</sub>S + (1-x)B<sub>2</sub>S<sub>3</sub> Glasses and Polycrystals by Multiple-Quantum MAS NMR of <sup>11</sup>B and <sup>23</sup>Na. *J. Am. Chem. Soc.* **1998**, *120*, 7337–7346.
- (50) Chen, L.; Zhang, M. J.; Yue, Y.; Ye, C. H.; Deng, F. Theoretical NMR Studies of Boron-Modified Mordenite. *Microporous Mesoporous Mater.* **2004**, *76*, 151–156.
- (51) Andronis, V.; Zografi, G. The Molecular Mobility of Supercooled Amorphous Indomethacin as a Function of Temperature and Relative Humidity. *Pharm. Res.* **1998**, *15*, 835–842.
- (52) Brus, J.; Urbanova, M. Selective Measurement of Heteronuclear <sup>1</sup>H–<sup>13</sup>C Dipolar Couplings in Motionally Heterogeneous Semicrystalline Polymer Systems. *J. Phys. Chem. A* **2005**, *109*, 5050–5054.